SELF-CONSISTENT FIELD THEORY SIMULATIONS OF WORMLIKE CHAINS ON CYLINDRICAL SURFACE

QIN LIANG, LU CHEN, HUI ZHANG, AND DONGLIANG ZHANG*

Abstract. Experimental investigation has shown that semiflexible polymers can wrap orderly around a cylinder. Recent Monte Carlo simulations also show that semiflexible polymers can develop linear or helical or random phase structures, depending on the rigidity or length of the polymer. Here, we use wormlike chain model and self-consistent field theory with Onsager interaction to study the micro-phase structure of polymers with local rigidity. We first give the modified diffusion equation for a wormlike chain on cylindrical surface, and then solve the equilibrium equations of the self-consistent field. A time splitting scheme is developed to solve the modified diffusion equation. However, only two kinds of nematic structures (N1 and N2) are detected in our simulation. In N1, the polymers are mainly oriented perpendicular to the axis of the cylinder; while in N2, the polymers are mainly oriented parallel to the axis of the cylinder. N1 is a metastable structure with free energy higher than N2.

Key words. wormlike chain model, modified diffusion equation, self-consistent field theory, cylindrical surface, micro-phase structure.

1. Introduction

Filaments with special chemical structure can spontaneously form a helical conformation such as some synthetic polymers [22] and biological materials like ds-DNA. And it has been shown that a filament with fully flexibility can also develop a helical conformation when it is bound to a deformable cylindrical surface [1]. For semiflexible polymers confined on the cylindrical surface, helical conformation could also be developed, for example, the arrangement of cellulose microfibrils in the plant cell wall [23]. Moreover, due to the rigidity of the polymer, this system is likely to form some liquid-crystal structures, such as nematic.

By using the Monte Carlo simulation, researchers [12, 17, 27] have studied the polymer wrapping of nanotubes. In the work of Gurevitch [12], the cylindrical surface-confinement was enforced by introducing the Lennard-Jones potential between the tube and the polymer particles. In additional to the bending potential between consecutive bonds, interactions between particles are also of Lennard-Jones type, which balances the attracting van der Waals force and the repelling force. All simulations [12, 17, 27] have maintained the existence of helical structures, which depends on the rigidity of the polymer and the radius of the tube. In these Monte carlo simulation, only one [17] or three [12] molecules are considered. That is because the computational cost depends on the number of polymers greatly. In the Monte Carlo methods, it is quite time-consuming to simulate systems of large molecule number and long contour length.

Self-consistent field theory (SCFT) is one of the common theories to study the micro-phase structure of polymers. It has achieved great success in dealing with flexible [7,11,15,20](Gaussian chain model) or semi-flexible [21,25] (wormlike chain

model) polymers. SCFT simplifies the many-body interactions to some field inter-
actions [9], hence is able to handle multi-chain systems. In this work, we use the
SCFT models with the excluded-volume Onsager interaction to study the phase
behavior of wormlike chains when confined on cylindrical surface.

In the self-consistent field model that based on the wormlike chain, a persistence
length λ is used to describe the rigidity of polymers. When $\lambda = \infty$, the polymers
are definitely hard; when $\lambda \ll 1$, the polymers are quite flexible. Therefore, the
wormlike model is able to cover systems of different rigidity. To simulate semiflexi-
ble systems with the self-consistent field theory (SCFT), it is of great importance to
write out and solve the modified diffusion equation (MDE) for the probability func-
tion of polymer chain statistics [9]. The MDEs in the cartesian coordinate system,
no matter it is for the Gaussian chain model dealing with the flexible polymers or
the wormlike chain model dealing with the semiflexible polymers, have both been
established decades ago [9,10]. Recently, the general MDE for the wormlike chain
in curvilinear coordinate system, particularly the MDE on the surface of sphere and
cylinder, has been deduced [18]. And the formulated MDE on a spherical surface
has been solved to study the nematic defect states of rigid linear particles confined
on a spherical surface [19]. Jeff [4] and Yang *et.al.* [26] have studied the confor-
mations of a single long flexible polymer when confined in the cylinder or on the
cylindrical surface by solving the long-polymer version of the MDE.

In the former theoretical work [18], although the MDE is given for any curvilinear
coordinate, the derivative terms are still written in the Cartesian coordinates form.
In this work, we first give the general self-consistent field model for wormlike chains
in the Cartesian coordinates. Then in section 3, we give the specific form of the
MDE, with all terms written in the curvilinear coordinate system. Two examples,
MDE in the spherical polar coordinates and the circular cylinder coordinates are
presented. SCFT equations for the wormlike chains confined on cylindrical surface
are listed in section 4. Here we only consider the simplified situation that the
functions are irrespective of the position. In section 5, details of the numerical
methods are listed. The time splitting method and Fourier spectral method are
used to solve the MDE, which is the most complicated equation in the SCFT model.
Picard mixing and the Anderson mixing schemes are applied to the updating of
the field. Section 6 deals with the numerical results. Although we expect the
wormlike chains to develop a helix on the surface of the cylinder. However, only
perpendicularly or parallelly oriented nematic structures (N1 and N2) are detected
in our simulation. In N1 the polymers are mainly oriented perpendicular to the
axis of the cylinder; while in N2 the polymers are mainly oriented parallel to the
axis of the cylinder. N1 is a metastable structure with free energy higher than N2.
In this section, comparison of N1 and N2 with the isotropic state are given. When
the length of the polymers approximates zero, this cylindrical confined system will
reduce to the two dimensional flat-plane system.

2. The general self-consistent field model for wormlike chains

The self-consistent field theory model is a mean field theory which treats the
many-body interaction of the molecules as a field interaction. In the SCFT frame,
finding the equilibrium state of the polymer system is to find the saddle point of
the free energy, which is a functional of the field function $W(\boldsymbol{r}, \boldsymbol{u})$ and the mean
segment density distribution $\rho(\boldsymbol{r}, \boldsymbol{u})$. [6,8,14] If we consider a system of n interacting
semiflexible polymer chains, with each chain has a contour length L and persistence

length λ, [9] then the free energy can be written as

$$
\begin{aligned}
\beta F(W, \rho) = \rho_0 \bigg[& \frac{C}{2} \int d\boldsymbol{r} \int d\boldsymbol{u} \int d\boldsymbol{u}' \rho(\boldsymbol{r}, \boldsymbol{u}) \rho(\boldsymbol{r}, \boldsymbol{u}') |\boldsymbol{u} \times \boldsymbol{u}'| \\
& - \int d\boldsymbol{r} \int d\boldsymbol{u} W(\boldsymbol{r}, \boldsymbol{u}) \rho(\boldsymbol{r}, \boldsymbol{u}) \bigg] - n \ln \left(\frac{Q(W)}{\rho_0} \right).
\end{aligned}
\tag{1}
$$

Here ρ_0 is the number density and C is the reduced molecular density. In three dimensional space, $\rho_0 = n/V$, with V being the volume of the system; the reduced molecular density $C = 2\rho_0 L^2 D$, with D being the diameter of polymers. In two dimensional surface, $\rho_0 = n/A$, with A being the area of the system; the reduced molecular density $C = \rho_0 L^2$. In Eq.(1), the dimensionless density distribution function ρ is normalized to the volume of the system, that is, in 3D, it satisfies

$$
\int d\boldsymbol{r} \int d\boldsymbol{u} \rho(\boldsymbol{r}, \boldsymbol{u}) = V.
\tag{2}
$$

Here $\boldsymbol{r}$ and $\boldsymbol{u}$ is the position and direction, respectively.

The Q in the last term of the free energy is the single chain partition function, which can be calculated by the so called propagator $q(\boldsymbol{r}, \boldsymbol{u}, s)$

$$
Q = \frac{1}{V} \int d\boldsymbol{r} \int d\boldsymbol{u} q(\boldsymbol{r}, \boldsymbol{u}, s = 1).
\tag{3}
$$

Note in Eq.(2) and (3), V should be changed to A in the surface case. The propagator q is defined for a polymer segment of length Ls, which represents the probability of finding the end located at a space point specified by $\boldsymbol{r}$ and pointing at a direction specified by $\boldsymbol{u}$. It satisfies a modified diffusion equation (MDE) [18].

$$
\begin{aligned}
\frac{\partial}{\partial s} q(\boldsymbol{r}, \boldsymbol{u}, s) \ = \ & \{ -W(\boldsymbol{r}, \boldsymbol{u}) - L\boldsymbol{u} \cdot \nabla_{\boldsymbol{r}} + L[(\boldsymbol{u} \cdot \nabla_{\boldsymbol{r}})\boldsymbol{u}] \cdot \nabla_{\boldsymbol{u}} \\
& + \frac{L}{2\lambda} \nabla_{\boldsymbol{u}}^2 \} q(\boldsymbol{r}, \boldsymbol{u}, s), \ \ s \in [0, 1], \\
& q(\boldsymbol{r}, \boldsymbol{u}, s = 0) = 1.
\end{aligned}
\tag{4}
$$

The first term of the right hand side is the field function. The second and the third terms are the convection terms. The third term is introduced by the locality of the coordinate system of $\boldsymbol{u}$. The last term is the diffusion terms introduced by the bending of polymers. When confined on surface, the last $\nabla_{\boldsymbol{u}}^2$ term should be split into

$$
\frac{L}{2\lambda} \nabla_{\boldsymbol{u}}^2 = -\frac{L\lambda}{2} \kappa^2(\boldsymbol{r}, \boldsymbol{u}) + \frac{L}{2\lambda} \frac{\partial^2}{\partial \varphi^2},
\tag{5}
$$

with φ being the on-plane angle that defines $\boldsymbol{u}$. The κ^2-term reflects the bending-energy penalty along the surface normal direction and the second term reflects the bending-energy penalty in the tangent plane. $\kappa(\boldsymbol{r}, \boldsymbol{u})$ is the surface curvature at position $\boldsymbol{r}$ and along the direction $\boldsymbol{u}$. It can be calculated by [5, 18]

$$
\kappa(\boldsymbol{r}, \boldsymbol{u}) = |[(\boldsymbol{u} \cdot \nabla_{\boldsymbol{r}})\boldsymbol{n}(\boldsymbol{r})] \times (\boldsymbol{u} \times \boldsymbol{n})|.
\tag{6}
$$

The vector $\boldsymbol{n}$ in the above equation is the unit normal vector of the surface.

Minimizing the free energy in Eq.(1) with respect to $\rho(\boldsymbol{r}, \boldsymbol{u})$ and $W(\boldsymbol{r}, \boldsymbol{u})$ leads to the self-consistent equations

$$(7) \qquad\qquad C \int \mathrm{d}\boldsymbol{u}' \rho(\boldsymbol{u}') |\boldsymbol{u} \times \boldsymbol{u}'| - W(\boldsymbol{u}) = 0,$$

$$(8) \qquad\qquad \rho(\boldsymbol{u}) = \frac{1}{Q} \int_0^1 \mathrm{d}s q(\boldsymbol{u}, s) q(-\boldsymbol{u}, 1-s).$$

Taking Eqs. (3),(4),(7) and (8), we then have a closed self-consistent set of equations for the calculation of $\rho(\mathbf{r}, \mathbf{u})$. Here the normalization condition in Eq.(2) is satisfied automatically by Eqs.(3) and (8).

3. The general expression of the MDE in orthogonal curvilinear coordinates

For some special system, it is more convenient to use some special curvilinear coordinates for the position $\boldsymbol{r}$ and use the corresponding local coordinates axes (changing with $\boldsymbol{r}$) for the direction $\boldsymbol{u}$. In this case, different curvilinear coordinates will results in different expressions of the MDE in Eq. (4), especially the gradient terms. In this section, we give the general expression of the MDE in any curvilinear coordinates. As for curvilinear coordinates, readers can refer to the book of Arfken and Weber [2](Chapter two). At the end of this section, several examples, both in the three dimension space or on the two dimension surface, are presented.

3.1. General expression. Suppose the position $\mathbf{r}$ is defined by some orthogonal curvilinear coordinates ξ_1, ξ_2, ξ_3 (i.e., Θ, Φ, r in spherical polar coordinate or ρ, φ, z in circular cylinder coordinates), then we define the natural basis vectors as

$$\mathbf{h}_i = \frac{\partial \boldsymbol{r}}{\partial \xi_i}, \ i = 1, 2, 3.$$

Note these vectors constitute a local basis that change their direction and/or magnitude from point to point. Let $h_i = |\mathbf{h}_i|$ be the length of $\mathbf{h}_i$ and then the local-normalized-curvilinear-orthonormal-basis-vectors can be defined

$$\mathbf{e}_i = \frac{\mathbf{h}_i}{h_i}, \ i = 1, 2, 3.$$

With these notifications, the gradient $\nabla_{\mathbf{r}}$ can be calculated [2]

$$(9) \qquad\qquad \nabla_{\mathbf{r}} = \mathbf{e}_1 \frac{1}{h_1} \frac{\partial}{\partial \xi_1} + \mathbf{e}_2 \frac{1}{h_2} \frac{\partial}{\partial \xi_2} + \mathbf{e}_3 \frac{1}{h_3} \frac{\partial}{\partial \xi_3}.$$

For fixed point $\boldsymbol{r}$, the local basis vectors $\mathbf{e}_i(\boldsymbol{r})$ are taken as the coordinate axis, and the orientation $\mathbf{u}$ of segments at this point can be represented by a spherical polar coordinates based on $\mathbf{e}_i, (i = 1, 2, 3)$[see FIGURE 1], that is,

$$(10) \qquad\qquad \mathbf{u} = \sin\theta \cos\varphi \mathbf{e}_1 + \sin\theta \sin\varphi \mathbf{e}_2 + \cos\theta \mathbf{e}_3.$$
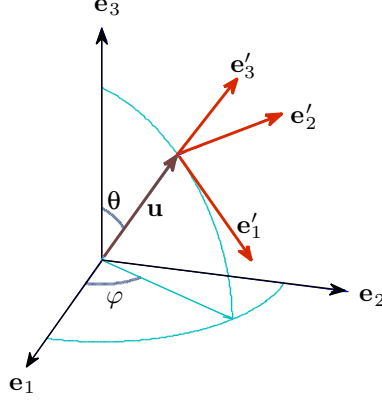
FIGURE 1. Schematics of the basis vectors for $\boldsymbol{u}$.

Now the local-normalized-curvilinear-orthonormal-basis-vectors for $\boldsymbol{u}$ are

(11)
$$
\begin{aligned}
\mathbf{e}_1' &= \cos\theta\cos\varphi\,\mathbf{e}_1 + \cos\theta\sin\varphi\,\mathbf{e}_2 - \sin\theta\,\mathbf{e}_3, \\
\mathbf{e}_2' &= -sin\varphi\,\mathbf{e}_1 + \cos\varphi\,\mathbf{e}_2, \\
\mathbf{e}_3' &= \sin\theta\cos\varphi\,\mathbf{e}_1 + \sin\theta\sin\varphi\,\mathbf{e}_2 + \cos\theta\,\mathbf{e}_3,
\end{aligned}
$$

Apply the similar equation of (9) to $\boldsymbol{u}$, $\nabla_{\mathbf{u}}$ can be calculated as

(12)
$$
\nabla_{\mathbf{u}} = \frac{\mathbf{e}_1'}{h_\theta}\frac{\partial}{\partial\theta} + \frac{\mathbf{e}_2'}{h_\varphi}\frac{\partial}{\partial\varphi} + \frac{\mathbf{e}_3'}{h_r}\frac{\partial}{\partial r}.
$$

As $\boldsymbol{u}$ is a unit vector with $r \equiv |\boldsymbol{u}| = 1$, the $\frac{\partial}{\partial r}$ term vanishes. In the spherical polar coordinates, $h_\theta = r = 1$, $h_\varphi = r\sin\theta = \sin\theta$, then the above gradient term can be simplified to

(13)
$$
\nabla_{\mathbf{u}} = \frac{\mathbf{e}_1'}{1}\frac{\partial}{\partial\theta} + \frac{\mathbf{e}_2'}{\sin\theta}\frac{\partial}{\partial\varphi}.
$$

Combining Eq. (9) and Eq. (10), we have

(14)
$$
\mathbf{u}\cdot\nabla_{\mathbf{r}} = \frac{\sin\theta\cos\varphi}{h_1}\frac{\partial}{\partial\xi_1} + \frac{\sin\theta\sin\varphi}{h_2}\frac{\partial}{\partial\xi_2} + \frac{\cos\theta}{h_3}\frac{\partial}{\partial\xi_3}.
$$

Substitute eqns. (10), (14), (13) into the term $[(\boldsymbol{u}\cdot\nabla_{\boldsymbol{r}})\boldsymbol{u}]\cdot\nabla_{\boldsymbol{u}}$ and use the partial derivative formula [2]

(15)
$$
\frac{\partial\mathbf{e}_i}{\partial\xi_j} = \mathbf{e}_j\frac{1}{h_i}\frac{\partial h_j}{\partial\xi_i}, \ (i\neq j) \ \frac{\partial\mathbf{e}_i}{\partial\xi_i} = -\sum_{j\neq i}\mathbf{e}_j\frac{1}{h_j}\frac{\partial h_i}{\partial\xi_j},
$$

we obtain the expression of the $[(\boldsymbol{u}\cdot\nabla_{\boldsymbol{r}})\boldsymbol{u}]\cdot\nabla_{\boldsymbol{u}}$ in the curvilinear coordinate form

(16)
$$
\begin{aligned}
&[(\boldsymbol{u}\cdot\nabla_{\boldsymbol{r}})\boldsymbol{u}]\cdot\nabla_{\boldsymbol{u}} \\
&= \left[\frac{\sin\theta\cos^2\varphi}{h_1 h_3}\frac{\partial h_1}{\partial\xi_3} - \frac{\cos\theta\cos\varphi}{h_1 h_3}\frac{\partial h_3}{\partial\xi_1} + \frac{\sin\theta\sin^2\varphi}{h_2 h_3}\frac{\partial h_2}{\partial\xi_3} - \frac{\cos\theta\sin\varphi}{h_2 h_3}\frac{\partial h_3}{\partial\xi_2}\right]\frac{\partial}{\partial\theta} \\
&+ \left[\cos\theta\sin\varphi\cos\varphi\left(\frac{1}{h_2 h_3}\frac{\partial h_2}{\partial\xi_3} - \frac{1}{h_1 h_3}\frac{\partial h_1}{\partial\xi_3}\right) + \frac{\cos^2\theta}{\sin\theta}\left(\frac{\sin\varphi}{h_1 h_3}\frac{\partial h_3}{\partial\xi_1} - \frac{\cos\varphi}{h_2 h_3}\frac{\partial h_3}{\partial\xi_2}\right)\right. \\
&\left. - \frac{\sin\theta\cos\varphi}{h_1 h_2}\frac{\partial h_1}{\partial\xi_2} + \frac{\sin\theta\sin\varphi}{h_1 h_2}\frac{\partial h_2}{\partial\xi_1}\right]\frac{\partial}{\partial\varphi}
\end{aligned}
$$

For the confined-on-surface case, supposing $\boldsymbol{u}$ lie on the plane spanned by $\mathbf{e}_1$ and $\mathbf{e}_2$ [see FIGURE 1], the above term can be simplified by setting $\theta \equiv \pi/2$ and $\frac{\partial}{\partial \theta} \equiv 0$, that is

$$(17) \qquad \left(\mathbf{u} \cdot \nabla_{\mathbf{r}}\right)\mathbf{u} \cdot \nabla_{\mathbf{u}} q(\mathbf{r}, \mathbf{u}, s) = \frac{1}{h_1 h_2}[\sin\varphi \frac{\partial h_2}{\partial \xi_1} - \cos\varphi \frac{\partial h_1}{\partial \xi_2}]\frac{\partial}{\partial \varphi} q.$$

As for the last term in Eq.(4), since $\boldsymbol{u}$ is represented by a spherical polar coordinates based on $\mathbf{e}_i$, the laplace term $\nabla_{\boldsymbol{u}}^2$ can be calculated as

$$(18) \qquad \nabla_{\boldsymbol{u}}^2 = \Big[\frac{1}{\sin\theta} \frac{\partial}{\partial \theta}\Big(\sin\theta \frac{\partial}{\partial \theta}\Big) + \frac{1}{\sin^2\theta} \frac{\partial^2}{\partial \varphi^2}\Big].$$

which is irrespective of the coordinates ξ_i.

Now the derivatives in Eq.(4) have been expressed in the curvilinear coordinates form in eqns. (14), (16), (18).

3.2. Examples for 3D space. In the following, we give three examples in 3D space with $\mathbf{r}$ defined in different coordinates: (i). Descartes coordinates; (ii). Spherical polar coordinates and (iii). Circular cylinder coordinates.

(i). Descartes coordinates

In descartes coordinates, $\xi_1 = x, \xi_2 = y, \xi_3 = z$, and $h_1 = h_2 = h_3 = 1$, derivatives in eqns. (14), (16) are

$$\mathbf{u} \cdot \nabla_{\mathbf{r}} = \sin\theta \cos\varphi \frac{\partial}{\partial x} + \sin\theta \sin\varphi \frac{\partial}{\partial y} + \cos\theta \frac{\partial}{\partial z},$$

$$[(\boldsymbol{u} \cdot \nabla_{\boldsymbol{r}})\boldsymbol{u}] \cdot \nabla_{\boldsymbol{u}} = 0.$$

(ii). Spherical polar coordinates.

In spherical polar coordinates, $\xi_1 = \Theta, \xi_2 = \Phi, \xi_3 = R$. Θ, Φ, R are the polar angle, the azimuth angle and the distance from the origin. The scale factors are $h_1 = R, h_2 = R\sin\Theta, h_3 = 1$, respectively. Derivatives in eqns. (14), (16) are

$$(19) \quad \begin{aligned} \mathbf{u} \cdot \nabla_{\mathbf{r}} &= \frac{\sin\theta \cos\varphi}{R} \frac{\partial}{\partial \Theta} + \frac{\sin\theta \sin\varphi}{R\sin\Theta} \frac{\partial}{\partial \Phi} + \frac{\cos\theta}{1} \frac{\partial}{\partial R}, \\ \left(\mathbf{u} \cdot \nabla_{\mathbf{r}}\right)\mathbf{u} \cdot \nabla_{\mathbf{u}} &= \frac{\sin\theta}{R} \frac{\partial}{\partial \theta} + \frac{\sin\theta \sin\varphi \cos\Theta}{R\sin\Theta} \frac{\partial}{\partial \varphi}. \end{aligned}$$

(iii). Circular cylinder coordinates.

Here $\xi_1 = \Phi, \xi_2 = z, \xi_3 = \rho$ and $h_1 = \rho, h_2 = 1, h_3 = 1$. Derivatives in eqns. (14), (16) are

$$(20) \quad \begin{aligned} \mathbf{u} \cdot \nabla_{\mathbf{r}} &= \frac{\sin\theta \cos\varphi}{\rho} \frac{\partial}{\partial \Phi} + \frac{\sin\theta \sin\varphi}{1} \frac{\partial}{\partial z} + \frac{\cos\theta}{1} \frac{\partial}{\partial \rho}, \\ \left(\mathbf{u} \cdot \nabla_{\mathbf{r}}\right)\mathbf{u} \cdot \nabla_{\mathbf{u}} &= \frac{\sin\theta \cos^2\varphi}{\rho} \frac{\partial}{\partial \theta} - \frac{\cos\varphi \cos\theta \sin\varphi}{\rho} \frac{\partial}{\partial \varphi}. \end{aligned}$$

Note the order of the coordinates can be modified as long as the $\mathbf{e}_1, \mathbf{e}_2, \mathbf{e}_3$ form a right-handed coordinate system. For example, in the circular cylinder coordinates, we can use $\xi_1 = \rho, \xi_2 = \Phi, \xi_3 = z$ and $h_1 = 1, h_2 = \rho, h_3 = 1$, then derivatives in eqns. (14), (16) can be written as

$$(21) \quad \begin{aligned} \mathbf{u} \cdot \nabla_{\mathbf{r}} &= \frac{\sin\theta \cos\varphi}{1} \frac{\partial}{\partial \rho} + \frac{\sin\theta \sin\varphi}{\rho} \frac{\partial}{\partial \Phi} + \frac{\cos\theta}{1} \frac{\partial}{\partial z}, \\ \left(\mathbf{u} \cdot \nabla_{\mathbf{r}}\right)\mathbf{u} \cdot \nabla_{\mathbf{u}} &= \frac{\sin\theta \sin\varphi}{\rho} \frac{\partial}{\partial \varphi}. \end{aligned}$$

which are different from those displayed in Eq. (20).

3.3. Examples for surface. Here we give two examples on surface with $\mathbf{r}$ confined on the : (i). spherical surface of radius R and (ii). cylinder surface of radius ρ. The derivatives for these cases can be achieved directly from the 3D issue by setting $\theta \equiv \pi/2, \dfrac{\partial}{\partial \theta} = 0$. In addition, the curvature κ should be calculated.

(i). Spherical surface of radius R

For spherical surface of radius R, derivatives in Eq.(19) can be written

$$
\begin{aligned}
\mathbf{u} \cdot \nabla_{\mathbf{r}} &= \frac{\cos \varphi}{R} \frac{\partial}{\partial \Theta} + \frac{\sin \varphi}{R \sin \Theta} \frac{\partial}{\partial \Phi}, \\
(\mathbf{u} \cdot \nabla_{\mathbf{r}}) \mathbf{u} \cdot \nabla_{\mathbf{u}} &= \frac{\sin \varphi \cos \Theta}{R \sin \Theta} \frac{\partial}{\partial \varphi}.
\end{aligned}
$$

(22)

and the curvature

$$
\begin{aligned}
\kappa(\mathbf{r}, \mathbf{u}) &= |[(\boldsymbol{u} \cdot \nabla_{\boldsymbol{r}}) \boldsymbol{n}(\boldsymbol{r})] \times (\boldsymbol{u} \times \boldsymbol{n})| \\
&= \left| \left(\frac{\cos \varphi}{R} \frac{\partial}{\partial \Theta} + \frac{\sin \varphi}{R \sin \Theta} \frac{\partial}{\partial \Phi} \right) \mathbf{e}_3 \times \left[(\cos \varphi \mathbf{e}_1 + \sin \varphi \mathbf{e}_2) \times \mathbf{e}_3) \right] \right| \\
&= \left| \left(\frac{\cos \varphi}{R} \mathbf{e}_1 + \frac{\sin \varphi}{R \sin \Theta} \sin \Theta \mathbf{e}_2 \right) \times (-\cos \varphi \mathbf{e}_2 + \sin \varphi \mathbf{e}_1)) \right| \\
&= \frac{1}{R}.
\end{aligned}
$$

(ii). Circular cylinder surface of radius ρ

For circular cylinder surface of radius ρ, derivatives in eqns. (20) can be written

$$
\begin{aligned}
\mathbf{u} \cdot \nabla_{\mathbf{r}} &= \frac{\cos \varphi}{\rho} \frac{\partial}{\partial \Phi} + \frac{\sin \varphi}{1} \frac{\partial}{\partial z}, \\
(\mathbf{u} \cdot \nabla_{\mathbf{r}}) \mathbf{u} \cdot \nabla_{\mathbf{u}} &= 0,
\end{aligned}
$$

(23)

and the curvature

$$
\begin{aligned}
\kappa(\mathbf{r}, \mathbf{u}) &= |[(\boldsymbol{u} \cdot \nabla_{\boldsymbol{r}}) \boldsymbol{n}(\boldsymbol{r})] \times (\boldsymbol{u} \times \boldsymbol{n})| \\
&= \left| \left(\frac{\cos \varphi}{\rho} \frac{\partial}{\partial \Phi} + \frac{\sin \varphi}{1} \frac{\partial}{\partial z} \right) \mathbf{e}_3 \times \left[(\cos \varphi \mathbf{e}_1 + \sin \varphi \mathbf{e}_2) \times \mathbf{e}_3) \right] \right| \\
&= \left| \left(\frac{\cos \varphi}{\rho} \mathbf{e}_1 \right) \times (-\cos \varphi \mathbf{e}_2 + \sin \varphi \mathbf{e}_1)) \right| \\
&= \frac{\cos^2 \varphi}{\rho}.
\end{aligned}
$$

(24)

4. SCFT of the wormlike chains on circular cylindrical surface

In order to investigate the wrapping conformations of wormlike chains around the circular cylindrical surface, we solve the corresponding SCFT equations in the circular cylindrical coordinates. In this section, we listed the SCFT equations that involved in our simulations.
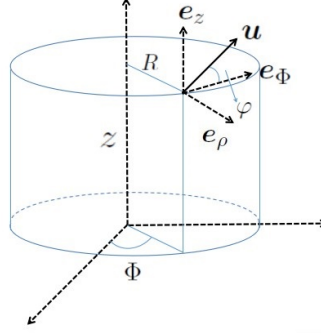
FIGURE 2. Schematics of the circular cylinder coordinates.

For this cylindrically confined system, the confinement includes two aspects. At first, the position $\boldsymbol{r}$ of segments should be located on the cylinder surface. Secondly, the direction $\boldsymbol{u}$ should be unit vector on the tangential plane of the cylinder surface. To enforce these two confinement, it is convenient to use the cylindrical coordinates. That is, the spatial variable $\boldsymbol{r}$ can be specified by two variables Φ, z, with $\Phi \in [0, 2\pi], z \in [0, H]$. For fixed position $\boldsymbol{r}$, the local coordinate bases of the cylindrical coordinate system are $\boldsymbol{e}_\Phi, \boldsymbol{e}_z, \boldsymbol{e}_\rho$, which is shown in Figure 2. Under this coordinate, $\boldsymbol{u}$ can be specified by an on-plane angle φ–the angle between $\boldsymbol{u}$ and $\boldsymbol{e}_\Phi$

$$(25) \qquad \boldsymbol{u} = cos\varphi \boldsymbol{e}_\Phi + sin\varphi \boldsymbol{e}_z.$$

Thus any functions $f(\boldsymbol{r}, \boldsymbol{u})$ can be written as $f(z, \Phi; \varphi)$ and the propagator can be expressed by these variables as $q(z, \Phi; \varphi; s)$.

Substitute the derivatives in Eq. (23-24) into the MDE of (4), we arrived at the final equation of the propagator

$$(26) \qquad \frac{\partial q}{\partial s} = -Wq - \frac{L\lambda}{2} \frac{cos^4\varphi}{R^2} q - \frac{L}{R} cos\varphi \frac{\partial q}{\partial \Phi} - Lsin\varphi \frac{\partial q}{\partial z} + \frac{L}{2\lambda} \frac{\partial^2 q}{\partial \varphi^2}.$$

In this simulation, we assume the distribution of the wormlike chain at any point of cylindrical surface is the same, the derivatives with respect to Φ and z in the modified diffusion equation vanish. Then we get

$$(27) \qquad \begin{aligned} &\frac{\partial q}{\partial s} = -Wq - \frac{L\lambda}{2} \frac{cos^4\varphi}{R^2} q + \frac{L}{2\lambda} \frac{\partial^2 q}{\partial \varphi^2}, \qquad \varphi \in [0, 2\pi], \quad s \in [0, 1], \\ &q(\varphi + 2\pi; s) = q(\varphi; s). \end{aligned}$$

The initial value of the propagator $q(\boldsymbol{u}, s)$ is 1, i.e.,

$$q(\varphi; 0) = 1.$$

The single chain partition function can be calculated through

$$(28) \qquad Q = \int_0^{2\pi} \mathrm{d}\varphi q(\boldsymbol{r}, \boldsymbol{u}, s = 1).$$

The equilibrium equations in Eqs. (7) and (8) also become

$$(29) \qquad W(\varphi) = C \int_0^{2\pi} \rho(\varphi') |\sin(\varphi - \varphi')| \mathrm{d}\varphi',$$

$$(30) \qquad \rho(\varphi) = \frac{1}{Q} \int_0^1 q(\varphi, s) q(\varphi + \pi, 1 - s) \mathrm{d}s.$$

Taking Eqs. (27),(28),(29) and (30), we then have a closed self-consistent set of equations for the calculation of $\rho(\varphi)$.

5. Numerical methods

In order to obtain the density distribution of the stable state, we have to solve the equations (27-30), which comprise a series of highly nonlinear equations or high order partial differential equations. Due to the strong nonlocality that emerges from the connection of propagators, density, and fields, it is difficult to solve these equations analytically. In this section, we present the numerical schemes for solving these equations. At first, the whole procedure to get the equilibrium state of this system is as follows:

Procedure A

> **step 1:** given some initial guess of the field function $W(\varphi)$.
> **step 2:** solve the modified diffusion equation in Eq. (27) to get $q(\varphi, s)$.
> **step 3:** obtain Q through the integration in Eq. (28), and the density $\rho(\varphi)$ through Eq. (30).
> **step 4:** update $W(\varphi)$ through Eq. (29).
> **step 5:** stop if $W(\varphi)$ converges (see Eq. (43)), otherwise go back to step2.

Generally, efficiency of the numerical method in solving the SCFT equations depends on three aspects:

> **1:** initial guess of the field function $W(\varphi)$;
> **2:** numerical schemes to solve the modified diffusion equation in (27);
> **3:** iterative method to update $W(\varphi)$.

5.1. Initial guess of W. As SCFT equations are a set of equations of multi-solutions, different initial field might result in different solution, or have different convergence rate. Hence suitable initial field is vital to the efficiency of the numerical method. For this simplified system (i.e., functions are irrespective of the position $\boldsymbol{r}$), we can use the isotropic state to get the initial guess of $W(\varphi)$. According to the normalization in Eq. (2),

$$\int d\boldsymbol{r} \int_0^{2\pi} d\boldsymbol{u} \rho(\boldsymbol{r}, \boldsymbol{u}) = A,$$

we can get

$$(31) \qquad \rho_i(\varphi) = \frac{1}{2\pi},$$

here the subscript i indicate isotropic. Substituting the above density into Eq. (29), the field function of the isotropic state can be obtained

$$(32) \qquad W_i(\varphi) = C \int_0^{2\pi} \rho_i(\varphi') |\sin(\varphi - \varphi')| \mathrm{d}\varphi' = C \int_0^{2\pi} \frac{1}{2\pi} |\sin(\varphi')| \mathrm{d}\varphi' = \frac{2C}{\pi},$$

which is the field function of the isotropic state that can be used as the initial guess of W.

5.2. Numerical method for solving the MDE. Among the whole procedure of this simulation, the most time consuming computation is the solving of the propagator. In this work, we split the right-hand side of Eq. (27) into two parts and treat the partial derivative term in the spectral space.

$$(33) \qquad O_1 q = -Wq - \frac{L\lambda}{2}\frac{cos^4\varphi}{R^2}q,$$

$$(34) \qquad O_2 q = \frac{L}{2\lambda}\frac{\partial^2 q}{\partial\varphi^2}.$$

the first operator O_1 is treated in the real space, and the second operator O_2 is treated in the spectral space. A second-order time splitting scheme is used. That is, for time step h

$$(35) \qquad q(\varphi; s+h) = e^{\frac{h}{2}O_1}e^{hO_2}e^{\frac{h}{2}O_1}q(\varphi; s).$$

Here the first operator, which is an ordinary differential operator, can be calculated exactly in the real space

$$(36) \qquad e^{\frac{h}{2}O_1}q(\varphi; s) = e^{-\frac{h}{2}W(\varphi)-\frac{h}{2}\cdot\frac{L\lambda}{2}\frac{cos^4\varphi}{R^2}}q(\varphi; s).$$

Due to the gradient terms, the second operator should be treated in the spectral space. We use Fourier spectral method [13]. The basic functions are

$$(37) \qquad \gamma_k(\varphi) = e^{ik\varphi}, \quad k \in \mathbb{Z}.$$

We can get

$$(38) \qquad O_2(\gamma_k) = -\frac{Lk^2}{2\lambda}\gamma_k, \quad k \in \mathbb{Z}.$$

Expanding the propagator in terms of the basic functions

$$q(\varphi; s) = \sum_k \hat{q}_k(s)\gamma_k(\varphi)$$

and solving the second operator in the spectral space

$$\frac{\partial q(\varphi; s)}{\partial s} = O_2(q).$$

We obtain

$$(39) \qquad \frac{\partial \hat{q}_k}{\partial s} = -\frac{Lk^2}{2\lambda}\hat{q}_k.$$

That is, for a time step h, we have

$$\hat{q}_k(s+h) = e^{-\frac{Lk^2}{2\lambda}h}\hat{q}_k(s).$$

Then we return to the real space and continue the calculation.

In the real space, we use N nodes for φ.

$$\varphi_j = \frac{2\pi}{N}j, \qquad j = 0, 1, ..., N-1.$$

The basis functions are $\gamma_k(k = -\frac{N}{2}, ..., \frac{N}{2})$.

5.3. Iterative method for the updating of W. To calculate the field through Eq. (29), one can use some numerical integration to implement the integral. Actually, this calculation can be easily implemented by using the spectral version of (29). That is, substituting the Fourier expansion of $\rho(\varphi')$

$$(40) \qquad \rho(\varphi') = \sum_k \hat{\rho}_k e^{ik\varphi'}$$

into Eq. (29), we have

$$
\begin{aligned}
W(\varphi) &= C \int_0^{2\pi} \rho(\varphi')|\sin(\varphi - \varphi')|\mathrm{d}\varphi' \\
&= C \int_0^{2\pi} \sum_k \hat{\rho}_k e^{ik\varphi'} |\sin(\varphi - \varphi')|\mathrm{d}\varphi' \\
(41) \qquad &= C \int_0^{2\pi} \sum_k \hat{\rho}_k e^{ik\varphi} e^{ik(\varphi'-\varphi)} |\sin(\varphi' - \varphi)|\mathrm{d}(\varphi' - \varphi) \\
&= C \sum_k \hat{\rho}_k e^{ik\varphi} \int_0^{2\pi} e^{ik\varphi'} |\sin(\varphi')|\mathrm{d}(\varphi') \\
&= C \sum_k \hat{\rho}_k e^{ik\varphi} \begin{cases} 0, \text{ for odd } k \\ -4/(k^2-1), \text{ for even } k \end{cases}.
\end{aligned}
$$

Hence, supposing the Fourier expansion of $W(\varphi)$ is

$$W(\varphi) = \sum_k \hat{W}_k e^{ik\varphi}$$

we have

$$(42) \qquad \hat{W}_k = \begin{cases} 0, \text{ for odd } k, \\ -\dfrac{4C}{k^2-1}\hat{\rho}_k, \text{ for even } k. \end{cases}$$

To update the field W, the simplest scheme is to directly replace the old field W_{old} with the new field W_{new}, which is arrived by Eq. (29). But this scheme is usually unstable. An alternative method is the Picard mixing method [7], which use the linear mixing of the old and new field

$$\alpha W_{\text{new}} + (1 - \alpha)W_{\text{old}}$$

as the renewed field function. Here α is usually set between $(0, 0.1)$ to ensure the stability of the iteration.

Recently, the Anderson mixing method [24] has been applied to SCFT simulations to update the field function. Anderson mixing method is a multi-step method designed to solve the fixed-point problem: $x = g(x)$. Here we list the **Anderson algorithm** as follows. Note in the following, $\mathbf{W}$ is a vector with $\mathbf{W} = (W(\varphi_0), W(\varphi_1), \cdots, W(\varphi_{N_1}))$. $\mathbf{G}(\mathbf{W}_{old})$ means the whole procedure by using the old field $\mathbf{W}_{old}$ to do **step 2** and **step 3** and obtain a renewed field through Eq. (29).

> Given initial guess $\mathbf{W}_0$ and $m \geq 1$,
> set $\mathbf{W}_1 = \mathbf{G}(\mathbf{W}_0)$.
> for $k = 1, 2, \cdots$
>   set $m_k = \min\{m, k\}$.
>   set $F_k = (\mathbf{f}_{k-m_k}, \cdots, \mathbf{f}_k)$, where $\mathbf{f}_i = \mathbf{G}(\mathbf{W}_i) - \mathbf{W}_i$.

Determine $\alpha^{(k)} = (\alpha_0^{(k)}, \cdots, \alpha_{m_k}^{(k)})^T$ that solves

$\min_{\alpha=(\alpha_0,\cdot,\alpha_{m_k})^T} ||F_k\alpha||$, s.t. $\sum\limits_{i=0}^{m_k} \alpha_i = 1$.

Set $\mathbf{W}_{k+1} = \sum\limits_{i=0}^{m_k} \alpha_i \mathbf{G}(\mathbf{W}_{k-m_k+i})$.

Note here F_k is a $N \times (m_k + 1)$ matrix. In our simulation, we use Picard iteration when the error is large, and use Anderson mixing when the error reduces below some threshold. In our simulation, we set the terminating criterion for W to be

$$(43) \qquad ||W_{new} - W_{old}|| := \frac{1}{N}\sqrt{\sum_{k=0}^{N-1}(W_{new}(\varphi_k) - W_{old}(\varphi_k))^2} < \epsilon = 10^{-5}.$$

6. Results

In this section, results of our simulations are presented. Since former work were done either by Monte Carlo simulation or by solving the simplified MDE for one or quite few (i.e., three) molecules, we haven't found any SCFT work for this cylindrical surface confined system. On the other hand, we have to confess that we don't detect helical conformations, which have been detected in Monte Carlo simulation. That might be due to the missing of the attracting interaction of the Onsager model, which only concludes compelling interaction. As is maintained in the work of Gurevitch [12] that the CH-π and the van der Waals interactions, which are all attracting interactions, are important for polymer wrapping. If we add some weakly attraction into the model, helix conformation might become stable. We will consider this in the future work. Here we only compare our work with the 2D flat plane case, which has only one kind of nematic structure. Moreover, as we are considering the simplified case, that is, the distribution is uniform in the position-space, only isotropic or nematic state (the helix structure can be regarded as one kind of nematic) can be found in our simulation.

At first, in order to compare the free energy of the simulated state with the isotropic state, we give the theoretical free energy of the isotropic in the 2D flat plane. Secondly, the theoretical isotropic-nematic transition for flat plane is presented. At last, results involving two nematic states (N1 and N2) and "isotropic" are given.

6.1. Free energy of the isotropic state. When $\frac{L}{R} \to 0$, the isotropic state (i.e., $\rho(\varphi) = const$) might be stable. In order to compare the free energy of the simulated state with the one of the isotropic state, we give the analytical free energy of isotropic state here. From Eq. (1), the free energy per polymer of this confined system can be written as

$$(44) \qquad \begin{aligned} \frac{\beta F(W,\rho)}{n} = &\left[\frac{C}{2}\int \mathrm{d}\varphi \int \mathrm{d}\varphi' \rho(\varphi)\rho(\varphi')|\sin(\varphi-\varphi')| \right. \\ &\left. - \int \mathrm{d}\varphi W(\varphi)\rho(\varphi) \right] - \ln\left(\frac{Q(W)}{\rho_0}\right). \end{aligned}$$

For field and density function that have achieved equilibrium (i.e., satisfying Eq. (29)), the free energy can also be calculated through

$$(45) \qquad E := \frac{\beta F(W,\rho)}{n} = -\frac{1}{2}\int_0^{2\pi} \mathrm{d}\varphi W(\varphi)\rho(\varphi) - \ln\left(\frac{Q(W)}{\rho_0}\right).$$

When $L \to 0$, from the SCFT equations (27-28) and the field for isotropic in (32), the propagate q and single partition function Q can be calculated

$$(46) \qquad q(\varphi, s) = e^{-Ws} = e^{-\frac{2Cs}{\pi}},$$

$$(47) \qquad Q = 2\pi e^{-\frac{2C}{\pi}}.$$

Substituting the density (31), the field (32) and the above Q into (44), the free energy of the isotropic state can be arrived

$$(48) \qquad E_{\text{ISO}} := \frac{\beta F_{iso}}{n} = -\frac{1}{2} \int_0^{2\pi} d\varphi \frac{2C}{\pi} \frac{1}{2\pi} - \ln\left(\frac{2\pi e^{-\frac{2C}{\pi}}}{\rho_0}\right) = \frac{C}{\pi} - \ln(\frac{2\pi}{\rho_0}).$$

6.2. Isotropic-nematic transition on two-dimensional flat plane. For an ideal two-dimensional flat semiflexible melts, there exists isotropic-nematic (I-N) transition. For the 2D flat system, the theoretical transition point C^* based on the Onsager model is [3, 16]

$$(49) \qquad C^*\left(\frac{L}{\lambda}\right) = \frac{3\pi(\frac{2L}{\lambda})^2}{4\left[\exp(-\frac{2L}{\lambda}) - 1 + \frac{2L}{\lambda}\right]}.$$

If we denote the free energy of the nematic state as E_N, then when $C > C^*$, $E_N < E_{\text{ISO}}$; pwhen $C < C^*$, $E_N \geq E_{\text{ISO}}$. Theoretically, when $\frac{L}{R} \to 0$, this cylindrically confined system will reduce to the ideal two-dimensional system. This means if we fix $\frac{L}{\lambda}$ and let $\frac{L}{R} \to 0$, we will encounter the I-N transition at C^*. However, for systems of positive L/R, the perfect isotropic state is not an equilibrium state of the current system (since function in (46) dose not satisfy the MDE (27)). Moreover, due to the non-vanishing curvature of the cylinder surface, polymers have to bend more than the ideal two-dimensional flat plane system, which results in a higher free energy. Hence for systems of small C, free energy is slightly larger than the free energy of isotropic state.

(a) N1   (b) N2
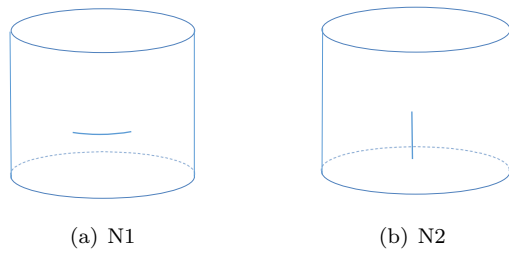
FIGURE 3. Schematics of nematic-1(N1) and nematic-2 (N2).

6.3. Two nematic states. From the SCFT equation (8), the density $\rho(\boldsymbol{u})$ is symmetric with $\rho(\boldsymbol{u}) = \rho(-\boldsymbol{u})$. In our system, this symmetry can be written as $\rho(\varphi) = \rho(\varphi + \pi)$. Moreover, from the definition of φ [see FIGURE 2], when the maximum of $\rho(\varphi)$ is arrived at 0 or π, the polymers are mainly oriented perpendicular to the axis of the cylinder (see FIGURE 3(a)). We call it a nematic-1 (N1) state. When the maximum of $\rho(\varphi)$ is arrived at $\pi/2$ or $3\pi/2$, the polymers are mainly oriented parallel to the axis of the cylinder (see FIGURE 3(b)). Both N1 and N2 can be detected (stable or metastable) in our simulation. However, the free energy of N1 is always larger than that of N2. This is because N2 has smaller

bending energy. Hence N1 is only a local minimum point not a global minimum point of the free energy.

In the following, we fix the length of the polymer $L/R = 0.1, 0.4, 0.8$, the persistence length $\lambda/L = 1$, and give a serials of free energy of N1 and N2 in FIGURE 4, FIGURE 5 and FIGURE 6. From the formula in (49), we see that the I-N transition point $C^* \approx 8.3$, which is marked with a dark green dot in these figures. In order to compare with the isotropic state of the ideal 2D flat plane, the free energy is subtracted with the free energy of the isotropic state in (48). We call it the relative energy. Moreover, we define the orientation order σ

$$\sigma = \int_0^{2\pi} \cos(2\varphi)\rho(\varphi)\mathrm{d}\varphi.$$

σ satisfies $-1 \leq \sigma \leq 1$. It yields a 0 value in the isotropic state, a positive value for N1 state and a negative value for N2 state. From the above definition, σ can also be calculated by $\sigma = 2\pi\hat{\rho}_2$, with $\hat{\rho}_k$ being the k-th Fourier coefficient (see Eq. (40)).

To get the initial guess of the field for N1 and N2 state, we use the Fourier expansion of W and the relation in (42)

$$
\begin{aligned}
W &= \hat{W}_0 + \hat{W}_2 \cos(2\varphi) \cdots \\
(50) \qquad &= \frac{2C}{\pi} - \frac{4C}{3}\hat{\rho}_2 \cos(2\varphi) \cdots \\
&= \frac{2C}{\pi} - \frac{4C}{6\pi}\sigma \cos(2\varphi) \cdots = \frac{2C}{\pi}\Big(1 - \frac{\sigma}{3}\cos(2\varphi)\cdots\Big).
\end{aligned}
$$

Therefor, we use

$$
\begin{aligned}
(51) \qquad W_{N1} &= \frac{2C}{\pi}\Big(1 - \frac{+1}{3}\cos(2\varphi)\Big) \\
W_{N2} &= \frac{2C}{\pi}\Big(1 - \frac{-1}{3}\cos(2\varphi)\Big)
\end{aligned}
$$

as the initial guess of W for N1 and N2 respectively.
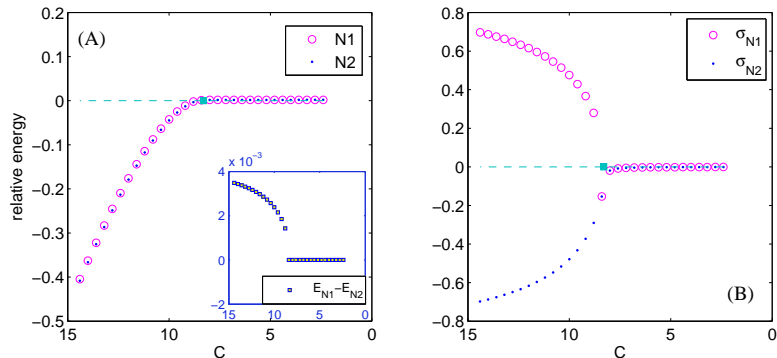
FIGURE 4. Results for $L/R = 0.1, \lambda/R = 0.1$. (A). Plot of relative free energy of N1 and N2 with decreasing C. The deep green dot here is the predicted I-N transition point in 2D flat plane. The subplot in (A) shows the energy difference $E_{N1} - E_{N2}$; (B). σ for N1 and N2.
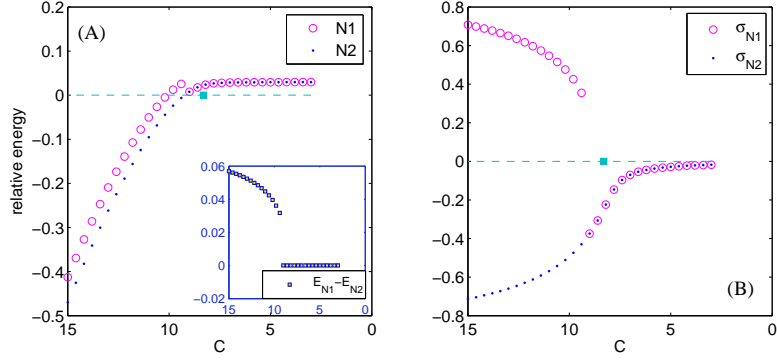
FIGURE 5. Results for $L/R = 0.4, \lambda/R = 0.4$. (A). Plot of relative free energy of N1 and N2 with decreasing C. The deep green dot here is the predicted I-N transition point in 2D flat plane. The subplot in (A) shows the energy difference $E_{N1} - E_{N2}$; (B). σ for N1 and N2.
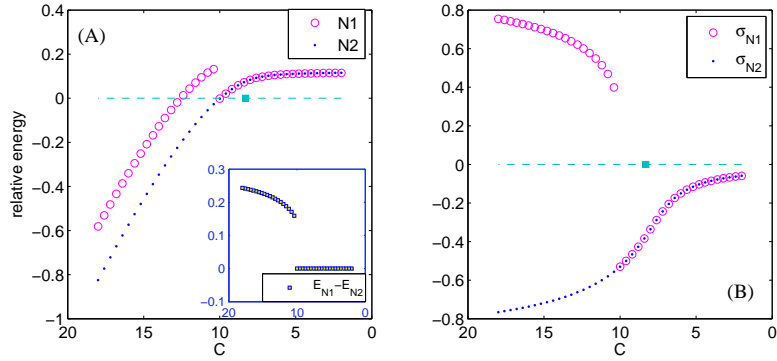
FIGURE 6. Results for $L/R = 0.8, \lambda/R = 0.8$. (A). Plot of relative free energy of N1 and N2 with decreasing C. The deep green dot here is the predicted I-N transition point in 2D flat plane. The subplot in (A) shows the energy difference $E_{N1} - E_{N2}$; (B). σ for N1 and N2.

6.3.1. Fix $L/R, \lambda/R$ and decrease C. When we fix $L/R, \lambda/R$, the nematic structure become more like a "isotropic" state (i.e., $\sigma = 0$) if C is decreased, especially in the small L/R case. As is mentioned above, when $L/R \to 0$, this cylindrically confined system will reduce to the ideal two-dimensional system. As shown in FIGURE 4, for short polymers (i.e., $L/R = 0.1$), the I-N transition point is almost the same with the one in ideal 2D flat system (marked by a dark green square). Moreover, difference between E_{N1} and E_{N2} is quite small (see the subplot in FIG-URE 4(A)). And when $C < C^*$, $E_{N2} - E_{ISO} \approx 0$. For small C, an N1 initial state will evolve into a N2 state (see the overlap of σ_{N1} and σ_{N2} when C is small), which means N1 is unstable here.

For long polymers, it is obvious that the relative energy $E_N - E_{ISO} > 0$ when $C < C^*$. This deviation from 0 is even bigger for larger L/R (see (A) of FIGURE

5 and FIGURE 6). It can be seen that when C is big, the energy of N1 is always larger than that of N2; when C is small, the N1 phase will also evolve into the N2 phase, which indicate the instability of N1.

6.3.2. Fix $L/R = 0.1, C = 10$ **and decrease** λ/R. Here we study the phase behavior of this confined system by fixing $L/R = 0.1, C = 10$ and changing the persistence length λ/R. Figures of the relative energy and the orientational order parameter are presented in FIGURE 7. Profiles of the density ρ for several persistence length are given in FIGURE 8. As is displayed in FIGURE 7, the persistence length do have impact on the phase behavior of this confined system. This is in accordance with the 2D flat situation. When λ/R approximate 0, the relative energy increases to 0 and the order parameter approaches 0, which is the feature of isotropic state. This can also be seen in FIGURE 8. In these simulations, the energy of N1 is also higher than the energy of N2. This energy difference is bigger for stiffer polymers.
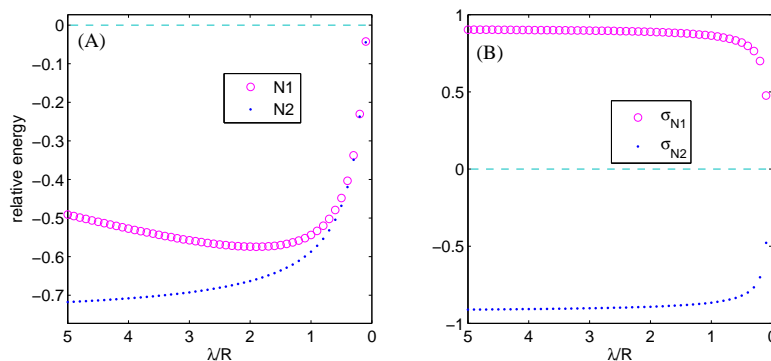
FIGURE 7. Results for $L/R = 0.1, C = 10$. (A). Plot of relative free energy of N1 and N2 with decreasing λ/R. (B). σ for N1 and N2.

(a) N1   (b) N2
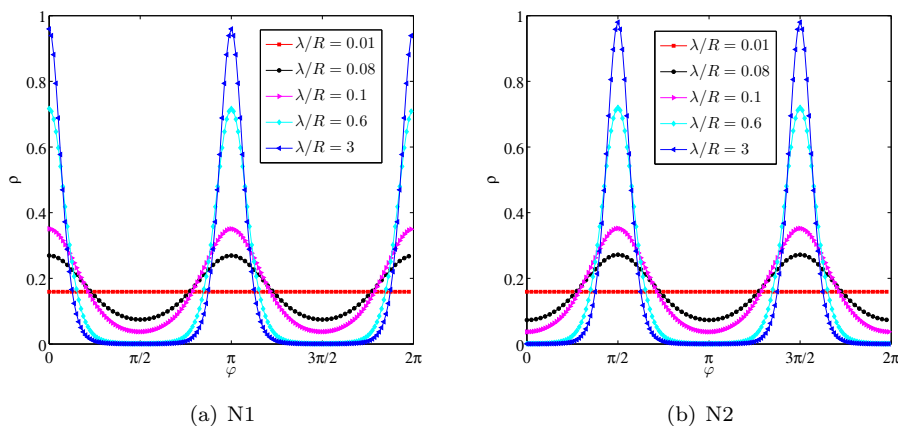
FIGURE 8. Profiles of density ρ for $C = 10, L/R = 0.1$ and different λ/R.

7. Conclusion

In this work, we give modified diffusion equation (MDE) of the wormlike chain in the curvilinear coordinate. Here all terms in the MDE are expressed in the curvilinear coordinate. With the MDE in the circular cylinder coordinates, we solved the SCFT equations on the circular cylinder surface to study the conformations of semiflexible polymer confined on the cylinder surface. A time splitting scheme is developed to solve the MDE. Different initial fields were designed to get different states. We didn't find the helical conformation but detected two kinds of nematic structures (N1 and N2) in our simulation. In N1 the polymers are mainly oriented perpendicular to the axis of the cylinder; while in N2 the polymers are mainly oriented parallel to the axis of the cylinder. N1 is a metastable structure with free energy higher than N2.

Acknowledgments

References

[1] A. Aric, J. C. Pamies and A. Cacciuto, Effective elasticity of a flexible filament bound to a deformable cylindrical surface, Phys Rev Lett, 104(22) (2010) 226101.

[2] G. B. Arfken, H. J. Weber and L. Ruby, Mathematical methods for physicists, Physics Today, 20(5) (2001) 79.

[3] J.Z.Y. Chen, Continuous isotropic-nematic transition of partially flexible polymers in two dimensions, Phys Rev Lett, 71(1) (1993) 93-96.

[4] J.Z.Y. Chen, Free energy and extension of a wormlike chain in tube confinement, Macromolecules, 46(24), (2013) 9837-9844.

[5] J.Z.Y. Chen, Theory of wormlike polymer chains in confinement, Prog Polym Sci, 54-55 (2016) 3-46.

[6] S. Cui, O. Akcakir and J.Z.Y. Chen, Isotropic-nematic interface of liquid-crystalline polymers, Phys Rev E, 51(1995) 4548-4557.

[7] F. Drolet, G.H. Fredrickson, Combinatorial screening of complex block copolymer assembly with self-consistent field theory, Phys Rev Lett, 83(21) (1999) 4317-4320.

[8] D.A.D.E. Dominik, Entropy-induced smectic phases in rod-coil copolymers, J Phys Cond. Matter, 14 (2002), arXiv:cond-mat/0205569.

[9] G.H. Fredrickson, The equilibrium theory of inhomogeneous polymers, Oxford University Press, USA, 2006.

[10] K.F. Freed, Functional integrals and polymer statistics, Adv Chem Phys, 22 (1972) 1-128.

[11] Z. Guo, G. Zhang, F. Qiu, H. Zhang, Y. Yang and A.C. Shi, Discovering ordered phases of block copolymers: New results from a generic Fourier-space approach, Phys Rev Lett, 101(2) (2008) 28301.

[12] I. Gurevitch and S. Srebnik, Monte Carlo simulation of polymer wrapping of nanotubes, Chem Phys Lett, 444(1) (2007) 96-100.

[13] H.Y. Li and L.L. Wang, A spectral method on tetrahedra using rational basis functions, Intern J Numer Anal Mod, 7(1) (2010) 330-355.

[14] Y. Jiang and J.Z.Y. Chen, Self-consistent field theory and numerical scheme for calculating the phase diagram of wormlike diblock copolymers, Phys Rev E Stat Nonl Soft Matter Phys, 88(4) (2013) 88042603.

[15] K. Jiang, Y. Huang and P.W. Zhang, Spectral method for exploring patterns of diblock copolymers, J Compt Phys, 229(20) (2010) 7796–7805.

[16] R.F. Kayser and H. J. Ravech, Bifurcation in Onsager's model of the isotropic-nematic transition, Phys Rev A, 17(6) (1978), 2067-2072.

[17] I. Kusner and S. Srebnik, Conformational behavior of semi-flexible polymers confined to a cylindrical surface, Chem Phys Lett, 430 (2006) 84-88.

[18] Q. Liang, J. Li, P.W. Zhang and J.Z.Y. Chen, Modified diffusion equation for the wormlike-chain statistics in curvilinear coordinates., J Chem Phys, 138(24) (2013) 1106.

[19] Q. Liang, S. Ye, P. Zhang and J.Z.Y. Chen, Rigid linear particles confined on a spherical surface: phase diagram of nematic defect states, J Chem Phys, 141(24) (2014) 244901.

[20] M.W. Matsen and M. Schick, Stable and unstable phases of a diblock copolymer melt, Phys Rev Lett, 72(16) (1994) 2660–2663.

[21] M.W. Matsen and C. Barrett, Liquid-crystalline behavior of rod-coil diblock copolymers, J Chem Phys, 109(10) (1998) 4108-4118.

[22] T. Nakano and Y. Okamoto, Synthetic helical polymers: conformation and function, Chem Rev, 101 (2001) 4013-4038.

[23] A. Neville, Biology of fibrous composites: development beyond the cell membrane, Cambridge University Press, 1993.

[24] H.F. Walker and P. Ni, Anderson acceleration for fixed-point iterations, SIAM J Numer Anal, 49(4) (2011) 1715-1735.

[25] V. Pryamitsyn and V. Ganesan, Self-assembly of rod-coil block copolymers, J Chem Phys, 120(12) (2004) 5824-5838.

[26] Y. Yang, T.W. Burkhardt and G. Gompper, Free energy and extension of a semiflexible polymer in cylindrical confining geometries, Phys Rev E, 76(1) (2007) 011804.

[27] D. Zhang, Z. Yang, X. Wen, Z. Xiang, L. He, S. Ran and L. Zhang, Helical conformations of semiflexible polymers confined between two concentric cylinders, J Phys Chem B, 115(49) (2011) 14333-14340.

Faculty of Mathematics and Computational Science, Xiangtan University, Xiangtan, Hunan, 411105, China
    E-mail: liangqin1997@xtu.edu.cn

School of Mathematical Sciences, Beijing Normal University, Beijing, 100875, China
    E-mail: nanbululu@mail.bnu.edu.cn

School of Mathematical Sciences, Laboratory of Mathematics and Complex Systems, Ministry of Education, Beijing Normal University, Beijing, 100875, China
    E-mail: hzhang@bnu.edu.cn

Beijing Orthodontics hospital, Capital Medical University, Beijing, 100006, China
    E-mail: zhangdongliang@hotmail.com